Published in final edited form as:
J Orthop Res. 2013 December ; 31(12): 2006–2012. doi:10.1002/jor.22449.

Histological Confirmation and Biological Significance of Cartilage Canals Demonstrated Using High Field MRI in Swine at Predilection Sites of Osteochondrosis

Ferenc Tóth[1], **Mikko J. Nissi**[2,3], **Jinjin Zhang**[2,3], **Michael Benson**[2,3], **Sebastian Schmitter**[2], **Jutta M. Ellermann**[2], and **Cathy S. Carlson**[1]

[1]Department of Veterinary Population Medicine, College of Veterinary Medicine, University of Minnesota, St. Paul, Minnesota

[2]Department of Radiology, Center for Magnetic Resonance Research, University of Minnesota, Minneapolis, Minnesota

[3]Department of Orthopaedic Surgery, University of Minnesota, Minneapolis, Minnesota

Abstract

Cartilage canal vessels in epiphyseal cartilage have a pivotal role in the pathogenesis of osteochondrosis/osteochondritis dissecans. The present study aimed to validate high field magnetic resonance imaging (MRI) methods to visualize these vessels in young pigs. Osteochondral samples from the distal femur and distal humerus (predilection sites of osteochondrosis) of piglets were imaged *post-mortem*: (1) using susceptibility-weighted imaging (SWI) in an MRI scanner, followed by histological evaluation; and (2) after barium perfusion using μCT, followed by clearing techniques. In addition, both stifle joints of a 25-day-old piglet were imaged in vivo using SWI and gadolinium enhanced T1-weighted MRI, after which distal femoral samples were harvested and evaluated using μCT and histology. Histological sections were compared to corresponding MRI slices, and three-dimensional visualizations of vessels identified using MRI were compared to those obtained using μCT and to the cleared specimens. Vessels contained in cartilage canals were identified using MRI, both ex vivo and in vivo; their locations matched those observed in the histological sections, μCT images, and cleared specimens of barium-perfused tissues. The ability to visualize cartilage canal blood vessels by MRI, without using a contrast agent, will allow future longitudinal studies to evaluate their role in developmental orthopedic disease.

Keywords

cartilage; cartilage canal; susceptibility weighted imaging; MRI; osteochondrosis

Cartilage canals are minute channels of vascularized mesenchyme that are present in the epiphyseal cartilage (chondroepiphysis) of the articular-epiphyseal cartilage complex

[*]*Correspondence to*: Ferenc Tóth (T: +1-612-624-7727; F: +1-612-624-3934; ftoth@umn.edu).

(AECC).[1–3] Vessels contained in the cartilage canals originate either from the dense plexus of vessels in the perichondrium or from the bone that forms the secondary center of ossification.[3,4] The primary function of these vessels is to provide nutrients to the epiphyseal cartilage. Cartilage canals also contribute to the formation and maintenance of the secondary ossification centers and contain perivascular mesenchymal cells, which provide a source of new chondrocytes.[3,5–7] As the individual ages and the epiphyseal cartilage decreases in thickness, cartilage canals disappear, either by incorporation into the advancing ossification front or via "chondrification," which is a physiologic process characterized by replacement of the blood vessels and stromal cells contained within the canal by chondrocytes.[4,7,8]

Damage to cartilage canals has been shown to be a key factor in the development of osteochondrosis (OC) in animals.[8–10] Histological studies evaluating joint cartilage samples obtained from predilection sites of OC in young horses,[8] swine,[7,10] and dogs[11] prior to the age at which clinical signs occur, demonstrate that failure of cartilage canal blood supply results in ischemic necrosis of the epiphyseal cartilage. This renders the overlying articular cartilage vulnerable to collapse, leading to formation of a chondral or osteochondral flap (osteochondritis dissecans). In addition, morphologic and histologic examination of human neonates affected by joint sepsis and osteomyelitis have demonstrated the role of cartilage canals in the extension of infection through the chondroepiphysis and into the secondary ossification centers.[12] It is highly likely that cartilage canal vessels are important in the pathogenesis of other developmental orthopedic diseases (e.g., hip/acetabular dysplasia); however, their potential role in human disease has largely been ignored. The most likely explanation for the paucity of human studies is that currently available imaging modalities do not allow for high quality imaging of cartilage canals, even with administration of a contrast medium. Application of novel imaging modalities capable of demonstrating cartilage canals contained in the AECC in vivo is needed to confirm or refute their role in human OC and other developmental orthopedic diseases and to follow the progression of the disease in animal studies.

In the study reported here, susceptibility-weighted imaging (SWI), a magnetic resonance imaging (MRI) sequence utilizing subtle differences in the magnetic susceptibilities of different tissues to generate contrast,[13,14] was used to demonstrate the presence and location of cartilage canals in porcine AECC. The image contrast in SWI is unique because it includes information from the phase data in addition to magnitude data. Thus, SWI is capable of depicting details potentially not visible using the standard proton density, T1 or T2 weighted imaging.[15]

The objectives of the study reported here were (1) to determine if cartilage canals in the AECC could be visualized in predilection sites of OC in young, healthy swine using non-contrast, susceptibility weighted MRI and (2) to compare the location and distribution of the cartilage canals visualized using SWI with those determined in vivo after injection of a standard contrast medium (gadolinium) and ex vivo using histological, tissue clearing, and μCT techniques. We hypothesized that vessels contained in the AECC could be demonstrated using SWI without administration of contrast media and that their location and architecture would match those observed in histological sections, cleared specimens or μCT.

Materials and Methods

Animals and Collection Procedures

The institutional animal care and use committee approved all procedures. For the ex vivo studies three swine, aged 1, 3, and 6 weeks, were anesthetized with telazole (10 mg/kg IM). Anesthetized swine were administered 500 IU/kg heparin intravenously, and then were euthanized using an overdose of pentobarbital. Immediately after euthanasia, the distal portions of the right femur and humerus were harvested and stored at –20°C for future MRI and histological evaluations. The left pelvic and thoracic limbs were left in situ and perfused with a 20% (v/v) solution of barium sulfate (Sol-O-Pake) in 10% neutral buffered formalin. Barium sulfate solution was administered using hand pressure from a 60 ml catheter tip syringe attached to a 6 French red rubber catheter inserted into the femoral artery or the axillary artery. Infusion of barium solution was continued until it leaked from the exposed veins. Upon completion of the perfusion, the distal third of each left humerus and femur was collected and stored at –20°C for future μCT evaluations. After completing the μCT imaging, barium perfused samples were cleared using the modified Spalteholz technique[16] to allow macroscopic visualization of the perfused cartilage canals.

For the in vivo study, anesthesia was induced in a 25-day-old piglet using telazole (10 mg/kg IM) and maintained by inhalation of isoflurane vaporized in oxygen. The stifle (knee) joints of the anesthetized piglet were imaged bilaterally in an MRI scanner using SWI and gadolinium enhanced T1-weighted MRI techniques. At the conclusion of the MRI studies, the piglet was heparinized and euthanized using identical methods to those described above. After collecting the right distal femur for histological processing, the left pelvic limb was perfused with barium, as described above, and the distal femur was harvested for μCT imaging.

MRI

Briefly, samples imaged ex vivo were allowed to thaw at room temperature prior to MRI scanning and were then immersed in Fluorinert to produce a clean background. A 9.4 T Agilent scanner with VnmrJ 3.1 and Varian volume transceiver RF coil was used for the scans. Susceptibility weighted imaging datasets were acquired using a three-dimensional (3D) gradient recalled echo sequence with repetition time of 40 ms, echo time of 14 ms and receiver bandwidth of 16 kHz. The field of view and imaging matrix were set for each sample to achieve approximately 100-μm isotropic resolution. SWI post processing was done according to Haacke et al.[15] To enhance visualization of the cartilage canals, 0.2-mm thick minimum intensity projections were calculated. Three-dimensional visualization of cartilage canals was created using OsiriX (Osirix v.5.0.2 32-bit, http://www.osirix-viewer.com).[17]

In vivo imaging studies were performed in a 7 T human whole body scanner (Magnetom 7T, Siemens, Erlangen, Germany) using an 8-channel transmit/receive knee coil (Virtumed, LLC, Minneapolis, MN) and a B1 shimming unit (CPC, Hauppauge, NY) with 8 × 1 kW amplifiers. Transmit B1 (B1+) phase shimming[18] was applied to achieve an appropriate flip angle homogeneity.[19,20] SWI scanning was performed using a 3-D GRE sequence with

manufacturer provided SWI-option enabled, including post-processing. The FOV was set as small as possible and an isotropic resolution of 0.25 mm^3 was reached. The acquisition parameters for SWI scan at 7 T were: TR = 27 ms, TE = 15 ms, receiver bandwidth = 90 Hz/pixel, nominal flip angle 15° and 3 averages. The total scan time with GRAPPA acceleration factor = 2 and partial Fourier acquisition was 22 min 41 s.

Upon conclusion of the SWI scanning, the pig was administered 0.2 mmol/kg gadolinium (Magnevist, Berlex Laboratories, Wayne, NJ) intravenously and imaged using a magnetization prepared turbo-FLASH (T1-weighted) 3D sequence approximately 3 min after administration of the contrast agent. The acquisition parameters were TR = 3,100 ms, TE = 3.6 ms, TI = 1,500 ms, bandwidth = 178 Hz/pixel and flip angle = 6°. The resolution was 0.55 mm^3 acquisition time 6 min 48 s.

Histology

At the conclusion of the MRI procedures, right femoral and humeral samples from the ex vivo study and the right distal femur from the in vivo study were placed in 10% neutral buffered formalin for 48 h followed by decalcification using 10% EDTA. Decalcified samples were cut into 2–3 mm thick slabs, which were then routinely processed into paraffin blocks. Two 5-μm thick sections each that were located 0, 50, 100, 150, and 200 μm below the surface of the block were obtained from selected blocks and stained with hematoxylin and eosin and toluidine blue. Individual slides were scanned at 2,400 dpi resolution (Epson Perfection V750-M Pro Scanner) and further processed using computer software (GIMP 2.8.3, http://www.gimp.org/). The two–five consecutive images, representing regions of samples 50–200 μm apart, were digitally summated/overlapped to improve the visualization of the 3D architecture of the vessels. The summated image of the consecutive sections was then compared with the corresponding MRI slice.

Selected sections immediately adjacent to those stained with toluidine blue were immunostained using an antibody directed against Von Willebrand Factor (Factor VIII-related antigen) to demonstrate endothelial cells in structures presumed to be cartilage canal vessels. Enzyme retrieval was achieved with Proteinase K (DAKO #S3020, Carpinteria, CA) and endogenous peroxidase was blocked with 3% hydrogen peroxide. Sections were incubated with universal protein block (DAKO #X0909) and then with 1:400 dilution of a polyclonal rabbit anti-human primary antibody directed against Von Willebrand Factor (DAKO #A0082), for 45 min. Binding of primary antibody was detected with DAKO Envision+ anti-rabbit HRP Polymer (DAKO #K4003) for 30 min. All sections were developed with DAB chromagen (DAKO #K3468) for 5 min and counterstained with Mayer's Hematoxylin (DAKO #S3302). For negative control slides the primary antibody was substituted with negative rabbit (DAKO #N1699) serum. Swine lung samples served as positive controls.

μCT

Barium sulfate-perfused left distal femora and humeri from the ex vivo study and the left distal femur from the in vivo study were allowed to thaw at room temperature, then were imaged using a Siemens Inveon preclinical μPET/CT scanner at 80 kV and 500 μA to obtain

a voxel resolution of 47.7 μm. Three-dimensional visualization of the barium sulfate perfused vessels contained in the cartilage canals was created using Osirix, similarly to the MRI 3D visualizations. Three-dimensional projections of the barium perfused vessels were visually compared to the 3D visualizations of the cartilage canals from SWI data of the contralateral limb for the ex vivo and in vivo studies.

Clearing of the Specimen

To allow macroscopic visualization of cartilage canals, barium perfused distal femora and humeri obtained in the ex vivo study were cleared using the modified Spalteholz technique[16] after the completion of the μCT imaging. Briefly, specimens were dehydrated by placing them into increasing concentrations of ethyl alcohol and then were cleared using concentrated methyl salicylate solution. Cleared specimens were photographed while immersed in methyl salicylate.

Results

Susceptibility weighted MRI consistently demonstrated cartilage canals present in the AECC, both ex vivo in disarticulated joint specimens and in vivo in intact joints. Barium-perfused vessels were clearly identified in μCT images, allowing for 3D reconstruction of the vascular architecture. Comparisons between histological sections (n = 2–5) that were summated into a single image and corresponding MRI slices revealed a close match between vessel profiles that were observed in the histological sections and those present in individual MR images in the ex vivo (Fig. 1) and in vivo (Fig. 2) studies, confirming the ability of the SWI technique to accurately identify cartilage canal vessels and demonstrating their localization at a lower magnetic field strength. Sections immunostained using an antibody directed against Von Willebrand Factor demonstrated the presence of endothelial cells within these structures, verifying their identity as cartilage canal vessels (Fig. 1).

In the ex vivo study, visual comparison between the cleared specimens and 3D reconstructions of μCT from the same limb, as well as with MR images obtained from the contralateral limb of the same individual, demonstrated a similar vascular architecture using all three techniques (Fig. 3). Further evaluation of these reconstructions revealed that visualization of vessels using the clearing method and μCT was largely limited to vessels arising from the perichondrium, whereas 3D images created from the MRI results readily demonstrated vessels arising from the perichondrium as well as vessels bridging the subchondral bone (Fig. 3). Vascularity and cartilage thickness decreased with age in both the distal femur and distal humerus.

Corresponding individual vessels were identified in the in vivo study when results of SWI were compared to images obtained after gadolinium contrast administration (Fig. 4), with the SWI having a superior resolution and ability to demonstrate the vasculature. Comparison of 3D visualizations of images obtained in the in vivo study using SWI at 7 T and μCT demonstrated a somewhat greater ability of μCT to resolve cartilage canals (Fig. 5).

Discussion

In this report, ex vivo and in vivo high resolution imaging of cartilage canals using non-contrast, high field, susceptibility weighted MRI was demonstrated. Our group is the first to compare images of the cartilage canals obtained using SWI to matching histological sections, and by doing so conclusively prove that structures observed in the MR images indeed correspond with the cartilage canals seen histologically.

Previously, imaging of cartilage canals has been attempted infrequently and has been limited to ex vivo, T2 weighted techniques[21] and in vivo use of gadolinium-enhanced MRI.[22] The resolution of the images obtained in those studies is insufficient to identify small avascular areas, such as those occurring in subclinical lesions of OC in animals, and, thus, appears to have limited potential for clinical utility. Our results using gadolinium contrast in the in vivo study demonstrated that, although it was possible to identify individual cartilage canals in the contrast enhanced images and their location corresponded with those seen in the SWI, the resolution and contrast-to-noise ratio between the vessels and surrounding matrix was vastly inferior to those achieved using SWI, likely due to the rapid extravasation of the gadolinium contrast agent.[22] With SWI, the deoxygenated blood likely present in the cartilage canals, both ex vivo and in vivo, results in a susceptibility difference between the cartilage canals and the surrounding matrix, generating a detectable phase difference between these tissues and yielding a contrast that appears more clear than that obtained using gadolinium.[15] An additional shortcoming of gadolinium contrast imaging is that the useful time for image acquisition after contrast administration is limited by the relatively rapid extravasation of the media. Furthermore, the gadolinium-enhanced imaging can only be repeated after a substantial time lag, first allowing for clearance of the extravascular contrast and then repeating its administration to ensure intravascular presence of gadolinium during the imaging.[22] Conversely, the contrast achieved with SWI is stable and does not depend on any exogenous agents, allowing for longer scanning times yielding a better signal-to-noise ratio. Importantly, gadolinium administration has also been associated with severe side effects, including nephrogenic systemic fibrosis.[23]

Comparison of the cleared specimens, μCT, and SWI visualization demonstrated good agreement between these modalities, all of which successfully identified cartilage canals in the ex vivo study. The processing of the 3-D visualizations, however, also revealed that working with the SWI contrast presents challenges because the contrast is negative and, thus, is highly similar to other regions of signal voids, such as bones, tendons, ligaments, and the overall image background. Despite this, SWI detected strikingly similar vessel architecture as compared to the μCT findings and cleared specimens. Furthermore, using SWI in the ex vivo study made it possible to detect vessels bridging the ossification front, whereas μCT and the clearing technique appeared to demonstrate only vessels arising from the perichondrium, in spite of the nominally higher resolution of the μCT (47 μm isotropic voxel size for μCT vs. ~100 μm for SWI). This disagreement was likely due to the inability of the radiocontrast media to adequately perfuse the vessels bridging the ossification front. This difference could be clinically important, since the ability of SWI to distinguish vessels within the subchondral bone may increase the likelihood that it will be a useful technique for the study of diseases known or suspected to involve the skeletal vasculature, such as

osteomyelitis and Legg–Perthes disease. Comparison of μCT and in vivo SWI results also revealed a closely similar architecture of the cartilage canals, but in this comparison the μCT appeared to provide superior resolution and contrast to noise ratio. This is likely due to the lower overall signal to noise ratio of the scanning configuration (coil size, sample size) at lower field strength (7 T), as well as the poorer resolution and shorter scanning time as compared to ex vivo at 9.4 T. Nevertheless, clinical use of contrast enhanced CT imaging for detection of cartilage canals is limited by the lower resolution of CT scanners used in clinical practice and the associated exposure to radiation, which is particularly concerning in children.

We believe that prospective in vivo use of SWI allowing visualization of cartilage canals will have multiple clinical applications. Failed vascular supply of the AECC is presumed to play an important role in the development of various diseases that affect both human beings and animals, including (but not limited to) OC, Legg–Perthes disease, and osteomyelitis.[7,8,10,11,24] Young piglets enrolled in the present study were free of orthopedic disease in order to determine if high field MRI techniques could identify cartilage canal vessels in normal tissues; however, future studies will be aimed at older pigs to identify both a vascular defect and changes in epiphyseal cartilage that are characteristic of chondronecrosis, a hallmark of OC. Studies designed to elucidate the role of cartilage canals in the development of OC in human beings are lacking, likely due to the fact that tissues from subclinical lesions are not available for evaluation and MRI techniques to identify cartilage canal vessels with the required precision have not been available. We propose that in situ/in vivo evaluation of cartilage canals at predilection sites of OC using the above described SWI method may help to clarify their role in the pathogenesis of human OC. In addition, identification of areas of the AECC with diminished blood supply may facilitate early diagnosis of human OC at a time when conservative treatment is more likely to succeed, and also (based on the size of the affected area) may improve the accuracy of determining whether or not an individual is a candidate for surgical treatment.[25] Similar to OC, the pathogenesis of Legg–Perthes disease, a condition characterized by ischemia of the capital femoral epiphysis in children, remains uncertain.[24] The ability to visualize changes in the blood supply of the AECC allowed by the SWI technique is expected to provide new information contributing to the better understanding of the pathogenesis of this condition. Imaging cartilage canals may also facilitate prognostication of septic arthritis/osteomyelitis by demonstrating the extent of cartilage canal involvement.

In conclusion, susceptibility weighted imaging of cartilage canals both ex vivo and in vivo allowed identification of cartilage canals in porcine distal femora and humeri at a resolution far exceeding that previously demonstrated. Although the present study was done at high magnetic field strengths (9.4 and 7 T), which have a limited clinical availability, preliminary studies comparing ex vivo results achieved using a 7 versus a 3 T magnet, which is commonly available clinically, are promising (unpublished data). In vivo application of this novel imaging modality will allow future longitudinal studies to evaluate the role of cartilage canal blood vessels in developmental orthopedic diseases such as, OC or Legg–Perthes disease.

Acknowledgments

The authors are grateful to Lynn Utecht and Dr Daniel Almeida for their assistance with the anesthetic procedures and to Dr Bruce Hammer for his help in obtaining μCT images. Support from grants T32OD010993, K18OD010468, P41 EB015894, S10 RR26783, R21 EB009138 and WM KECK Foundation were used during the completion of the study. None of the authors had any competing interests pertaining to this manuscript.

References

1. Blumer MJ, Longato S, Richter E, et al. The role of cartilage canals in endochondral and perichondral bone formation: are there similarities between these two processes? J Anat. 2005; 206:359–372. [PubMed: 15817104]
2. Visco DM, Van Sickle DC, Hill MA, et al. The vascular supply of the chondro-epiphyses of the elbow joint in young swine. J Anat. 1989; 163:215–229. [PubMed: 2606774]
3. Wilsman NJ, Van Sickle DC. Cartilage canals, their morphology and distribution. Anat Rec. 1972; 173:79–93. [PubMed: 5028066]
4. Olstad K, Ytrehus B, Ekman S, et al. Epiphyseal cartilage canal blood supply to the distal femur of foals. Equine Vet J. 2008; 40:433–439. [PubMed: 18487109]
5. Haines RW. Cartilage canals. J Anat. 1933; 68:45–64. [PubMed: 17104463]
6. Visco DM, Hill MA, Van Sickle DC, et al. The development of centres of ossification of bones forming elbow joints in young swine. J Anat. 1990; 171:25–39. [PubMed: 2081708]
7. Ytrehus B, Ekman S, Carlson CS, et al. Focal changes in blood supply during normal epiphyseal growth are central in the pathogenesis of osteochondrosis in pigs. Bone. 2004; 35:1294–1306. [PubMed: 15589210]
8. Olstad K, Ytrehus B, Ekman S, et al. Epiphyseal cartilage canal blood supply to the tarsus of foals and relationship to osteochondrosis. Equine Vet J. 2008; 40:30–39. [PubMed: 18083657]
9. Carlson CS, Cullins LD, Meuten DJ. Osteochondrosis of the articular-epiphyseal cartilage complex in young horses: evidence for a defect in cartilage canal blood supply. Vet Pathol. 1995; 32:641–647. [PubMed: 8592799]
10. Carlson CS, Hilley HD, Meuten DJ. Degeneration of cartilage canal vessels associated with lesions of osteochondrosis in swine. Vet Pathol. 1989; 26:47–54. [PubMed: 2913703]
11. Weiss S, Loeffler K. Histological study of cartilage channels in the epiphyseal cartilage of young dogs and their relationship to that of osteochondrosis dissecans in the most frequently affected locations. DTW Dtsch Tierarztl Wochenschr. 1996; 103:164–169. [PubMed: 8964237]
12. Ogden JA. Pediatric osteomyelitis and septic arthritis: the pathology of neonatal disease. Yale J Biol Med. 1979; 52:423–448. [PubMed: 524924]
13. Reichenbach JR, Venkatesan R, Schillinger DJ, et al. Small vessels in the human brain: MR venography with deoxyhemoglobin as an intrinsic contrast agent. Radiology. 1997; 204:272–277. [PubMed: 9205259]
14. Haacke EM, Xu Y, Cheng YC, et al. Susceptibility weighted imaging (SWI). Magn Reson Med. 2004; 52:612–618. [PubMed: 15334582]
15. Haacke EM, Mittal S, Wu Z, et al. Susceptibility-weighted imaging: technical aspects and clinical applications, part 1. Am J Neuroradiol. 2009; 30:19–30. [PubMed: 19039041]
16. Guyer, MF. Practical exercises in zoological micro-technique. 5th ed.. University of Chicago Press; Chicago, IL: 1953. Objects of general interest. In: Animal micrology.; p. 110-113.
17. Rosset A, Spadola L, Ratib O. OsiriX: an open-source software for navigating in multidimensional DICOM images. J Digit Imaging. 2004; 17:205–216. [PubMed: 15534753]
18. Metzger GJ, Auerbach EJ, Akgun C, et al. Dynamically applied B(1) (+) shimming solutions for non-contrast enhanced renal angiography at 7.0 Tesla. Magn Reson Med. 2013; 69:114–126. [PubMed: 22442056]
19. Van de Moortele PF, Akgun C, Adriany G, et al. B(1) destructive interferences and spatial phase patterns at 7 T with a head transceiver array coil. Magn Reson Med. 2005; 54:1503–1518. [PubMed: 16270333]

20. Ellermann J, Goerke U, Morgan P, et al. Simultaneous bilateral hip joint imaging at 7 Tesla using fast transmit B (1) shimming methods and multichannel transmission—A feasibility study. NMR Biomed. 2012; 25:1202–1208. [PubMed: 22311346]

21. Babyn PS, Kim HK, Lemaire C, et al. High-resolution magnetic resonance imaging of normal porcine cartilaginous epiphyseal maturation. J Magn Reson Imaging. 1996; 6:172–179. [PubMed: 8851424]

22. Jaramillo D, Villegas-Medina OL, Doty DK, et al. Age-related vascular changes in the epiphysis, physis, and metaphysis: normal findings on gadolinium-enhanced MRI of piglets. Am J Roentgenol. 2004; 182:353–360. [PubMed: 14736661]

23. Kuo PH, Kanal E, Abu-Alfa AK, et al. Gadolinium-based MR contrast agents and nephrogenic systemic fibrosis. Radiology. 2007; 242:647–649. [PubMed: 17213364]

24. Hresko MT, McDougall PA, Gorlin JB, et al. Prospective reevaluation of the association between thrombotic diathesis and Legg–Perthes disease. J Bone Joint Surg Am. 2002; 84-A:1613–1618. [PubMed: 12208918]

25. Kocher MS, Czarnecki JJ, Andersen JS, et al. Internal fixation of juvenile osteochondritis dissecans lesions of the knee. Am J Sports Med. 2007; 35:712–718. [PubMed: 17337729]

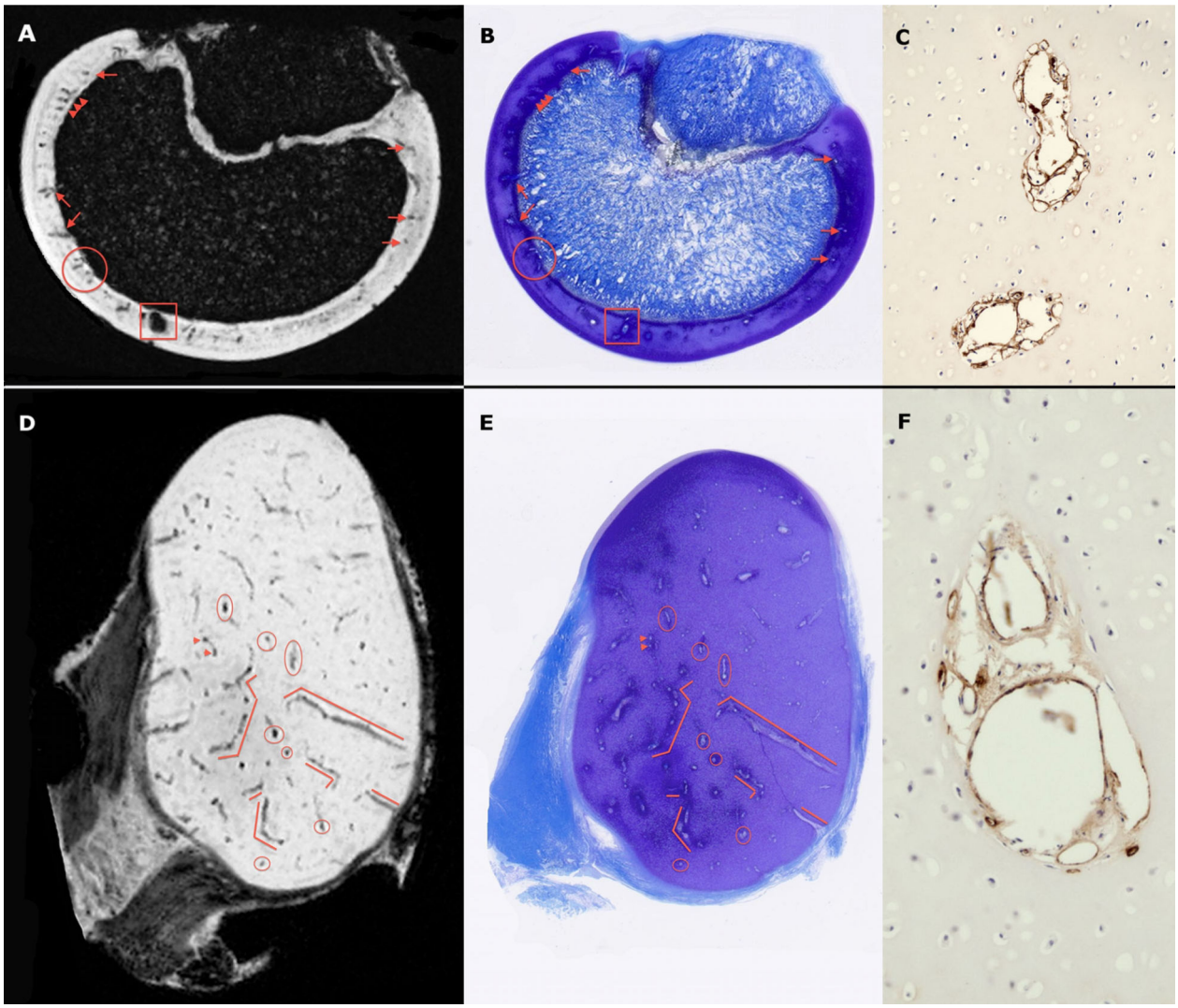

Figure 1.

Ex vivo SWI images (Panels A and D) obtained using a 9.4 T MRI scanner and corresponding toluidine blue stained histological slides (panels B and E) of the sagittal ridge of the humeral trochlea of a 6-week-old pig (upper panels, sectioned in the sagittal plane) and medial femoral condyle of a 3-week-old pig (lower panels, sectioned in the transverse plane). Red markers identify corresponding cartilage canal vessels. Immunostaining of adjacent sections using an antibody directed against Von Willebrand Factor (Panels C and F; imaged with a 20× objective) demonstrated positive immunostaining (brown reaction product) in endothelial cells lining cartilage canal vessels.

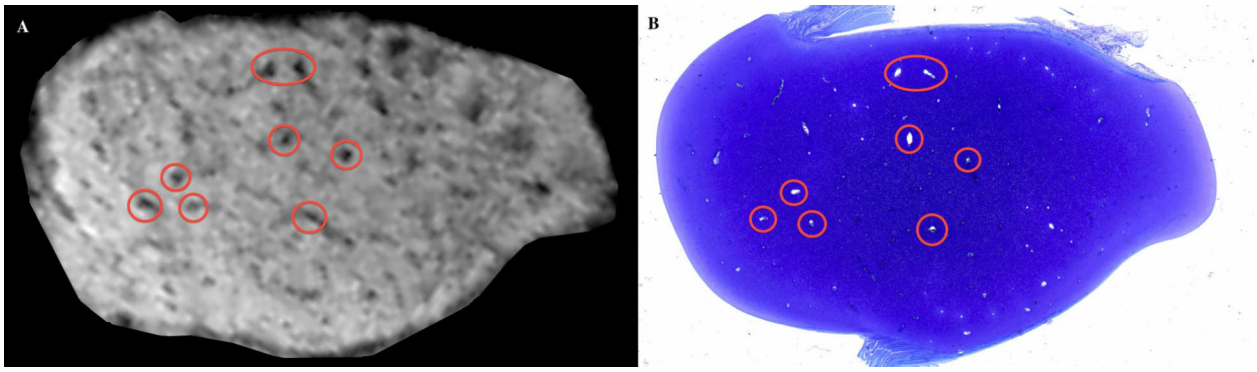

Figure 2.

In vivo SWI image (left panel) obtained with a 7 T MRI scanner and corresponding toluidine blue stained histological slide (right panel) of a transverse plane section of the medial femoral condyle of a 25-day-old pig. Red circles identify matching cartilage canal vessels.

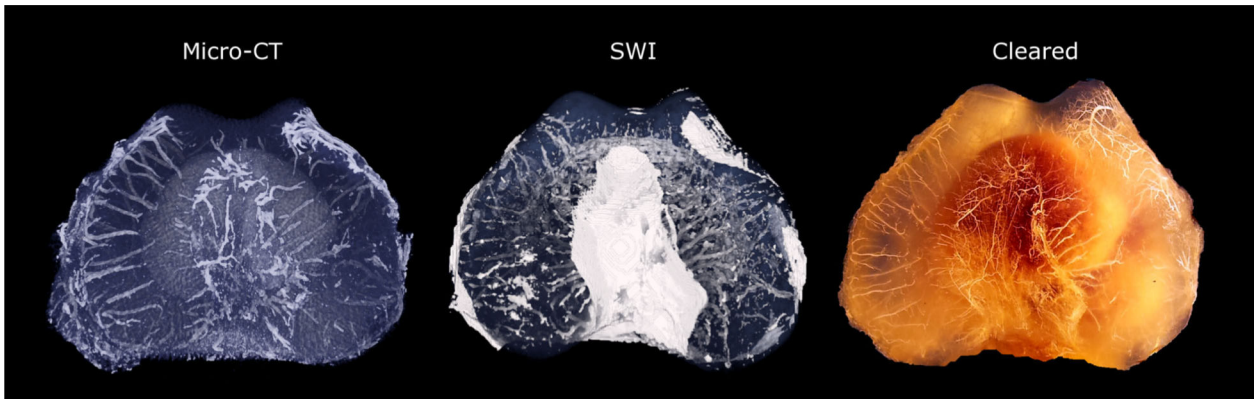

Figure 3.

Corresponding three-dimensional visualizations of the ex vivo SWI (middle panel), barium perfused μCT (left panel) images and the barium perfused and cleared specimen (right panel) of the distal aspect of the femur of a 1-week-old pig demonstrating similar architecture of the cartilage canal vessels. The SWI data were obtained from the right limb using a 9.4 T MRI scanner whereas the μCT and clearing procedures were performed on the left limb.

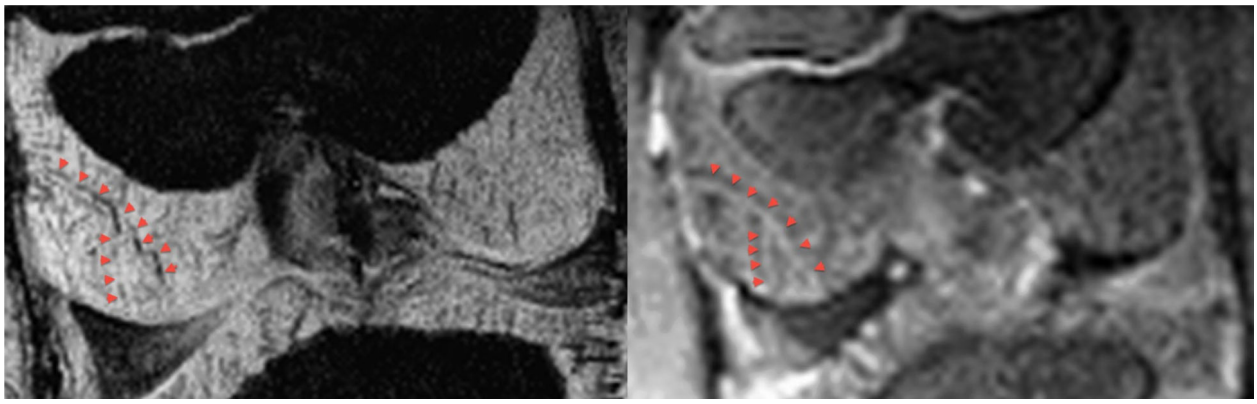

Figure 4.

The same cartilage canal vessel (red arrowheads) as seen in an in vivo SWI image (left panel) and corresponding gadolinium contrast enhanced (right panel) coronal plane image of the distal femur of a 25-day-old pig. Images were obtained using a 7 T MRI scanner.

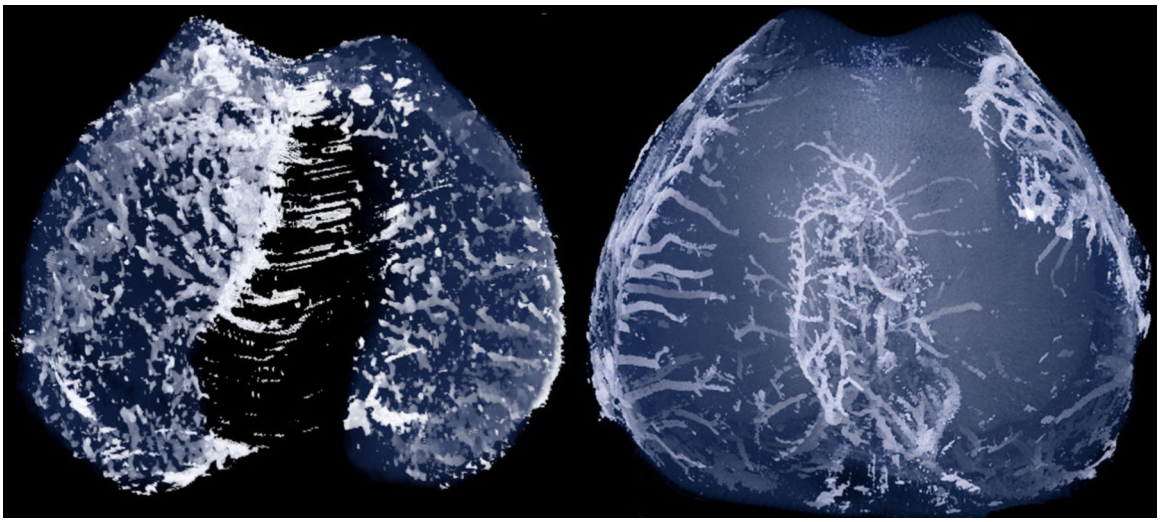

Figure 5.

Corresponding projections of three-dimensional visualizations of in vivo SWI obtained using a 7 T MRI scanner (left panel, AECC manually segmented for 3-D visualization) and ex vivo barium perfused μCT (right panel) images of the distal femur of a 25-day-old pig.